Eur. Phys. J. B **23**, 17–28 (2001)

THE EUROPEAN PHYSICAL JOURNAL B

EDP Sciences

Micromagnetic structure in multilayer films with moderate perpendicular anisotropy

M. Labrune[1,a] and A. Thiaville[2]

[1] Laboratoire PMTM, Institut Galilée, Université Paris 13, 93430 Villetaneuse, France
[2] Laboratoire de Physique des Solides, CNRS - Université Paris-Sud, 91405 Orsay, France

Received 12 January 2001 and Received in final form 15 May 2001

Abstract. Micromagnetic simulations have been performed in order to obtain deeper insight into the domain structures within multilayer films, as they are expected to differ from those of single films. These 2D calculations have been done in the case of multilayers exhibiting a moderate perpendicular anisotropy, with no indirect exchange coupling between the magnetic layers, where a "weak stripe" domain structure develops. First, these results are compared quantitatively to the very detailed experimental data available in the literature on the $(Co/Au)_N$ system. More generally, the nucleation of a stripe pattern in multilayers is discussed as a function of the magnetic parameters and the number of magnetic layers in the stack. Compared to a single film, two main differences appear in the equilibrium domain period and the magnetization profiles. The physical origin of these effects is discussed.

PACS. 75.60.Ch Domain walls and domain structure – 75.70.Cn Interfacial magnetic properties (multilayers, superlattices) – 75.50.Ss Magnetic recording materials

1 Introduction

Materials with an artificial layered structure consisting of alternating ferromagnetic and non ferromagnetic films have received considerable attention due to their novel magnetic properties. When the magnetic films in the stack are composed of Co (or Ni), a perpendicular anisotropy can develop. Therefore, such multilayers are attractive candidates to magneto-optical technology. To obtain deeper insight in this kind of system it is important to know its micromagnetic properties, which obviously differ from those of single films. Only few results on micromagnetic simulations are available in the literature, always closely associated to experimental investigation of domain structures in Co/Pt or Co/Pd multilayers by Lorentz transmission electron microscopy [1], magnetic force microscopy [2,3] and Bitter pattern [4]. Thus, no general understanding of the peculiarities of the micromagnetic structures in multilayers has been proposed up to now, especially in the regime of moderate anisotropy. In this case indeed, the traditional separation of the structure into well-defined domains and domain walls of fixed energy is not relevant, the magnetic structure being rather described by a continuous rotation of magnetization.

The motivation of the present study starts with the publication of new experimental results [5–7] on the change of micromagnetic structure in cobalt-gold multilayer films (Fig. 1) with perpendicular anisotropy, according to the number of magnetic layers in the stack. These authors [5–7] investigated the depth dependent magnetization orientation by locally doping the Co layers with ^{57}Fe Mössbauer probes. The [Co(20 Å)/Au(20 Å)] samples were elaborated by ultrahigh vacuum deposition. ^{57}Fe Mössbauer probe layers with nominal thickness of one angström, which corresponds to about half an atomic layer, were inserted into the middle of the cobalt layers.

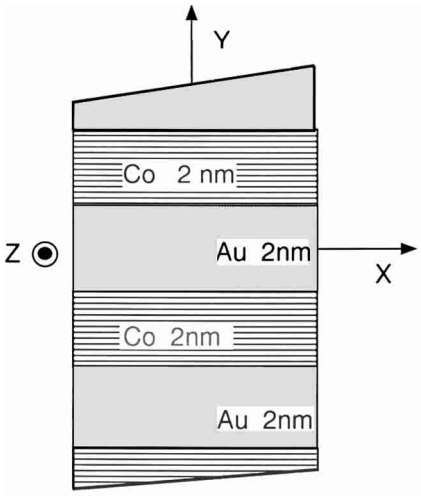

Fig. 1. Multilayer geometry investigated in this work. The c-axis of the cobalt layers is always along the surface normal (Y).

[a] e-mail: ml@lpmtm.univ-paris13.fr

Table 1. Depth-dependent Mössbauer parameters for $N = 31$. The error on $\overline{H}_{\rm d}$ is estimated to be ± 2 kOe (from Refs. [6,7]).

Probe position	Layers 1–5	Layers 6–10	Layers 11–20	Layers 22–26	Layers 27–31
$\overline{H}_{\rm d}$ (kOe)	0	–4	–6	–3	0
$\bar{\theta}$ (deg.)	57°	36°	28°	30°	46°

For some samples all the cobalt layers contained the iron probe whereas for others only a few layers in the stack did. The average angle $\bar{\theta} = A\cos(\sqrt{\langle\cos^2\theta\rangle})$ of the iron moment vectors can be deduced from the analysis of the Mössbauer spectra, where θ is the angle between an iron moment vector and the normal to the stack. Assuming that the iron moments are strongly coupled ferromagnetically with the surrounding cobalt ones, the average magnetization direction of the probed magnetic layers may be obtained. The variation of the average angle $\bar{\theta}$ throughout the N magnetic layers in the stack as a function of N was given in references [6,7]. The $\bar{\theta}(N)$ variation indicates that, in spite of a perpendicular anisotropy, for a moderate number of magnetic layers in the stack, the magnetization vector is mainly in-plane. However, when increasing N, the out-of-plane component gradually increases. A "spin reorientation transition" from in-plane to out-of-plane is then observed. Such a situation recalls the magnetic behavior of ultra-thin films exhibiting perpendicular anisotropy where beyond a critical thickness the magnetization starts to deviate from the in-plane uniformly magnetized state, oscillating periodically [8,9]. This analysis was confirmed by VSM measurements showing the decrease of the in-plane remanent magnetization $M_{\rm R}$ with increasing N, and also by magnetic force microscopy (MFM) observations [7] where for $N \geq 8$ stripe domains are clearly visible. Finally, in the particular case $N = 31$, series of multilayers were prepared to examine the depth dependence of the micromagnetic structure in the Co layers. In each stack, only five Co layers out of 31 were doped with ^{57}Fe. These five layer blocks were located at different levels in the stack according to various samples in the series (see Fig. 2). The Mössbauer results showed that $\bar{\theta}$ is much higher near the external surfaces, that is the magnetization is more in-plane than in the middle of the stack, where a pronounced component normal to the film plane exists. Furthermore, the average demagnetizing field component along the magnetization direction could be extracted from the Mössbauer spectra [6,7]. These values are gathered in Table 1.

The present communication aims first at comparing these available experimental results to numerical simulations. Then, this analysis is extended to the study of the ripening (development) of stripe domains in multilayers with N as a parameter, in order to highlight the basic differences between multilayers and single films. All calculations consider the moderate anisotropy case ($Q = K/2\pi M_{\rm S}^2 < 1$), where for a single magnetic layer the magnetization would lie parallel to the film plane.

The bases of the numerical method are outlined in Section 2. A full description of the equilibrium magnetic configuration found in zero field for $N = 31$ magnetic layers is provided in Section 3 and compared to the corresponding experimental results. In Section 4, numerical predictions concerning the type of magnetic structure and the relative magnetic parameters ($\bar{\theta}$, $M_{\rm R}$ and domain width W) as a function of N are obtained and compared to the available experimental data. Finally in Section 5, the nucleation of a stripe domains in multilayers is analysed according to the number of magnetic layers in the stack and the value of the perpendicular uniaxial anisotropy, keeping $Q < 1$. In that section, the evolution of the remanent magnetization $M_{\rm R}$ (the value of magnetization at zero field, for a field applied in-plane and along the stripes – the longitudinal direction), but also a local description of $\mathbf{m}$, will be shown during the ripening of stripe domains.

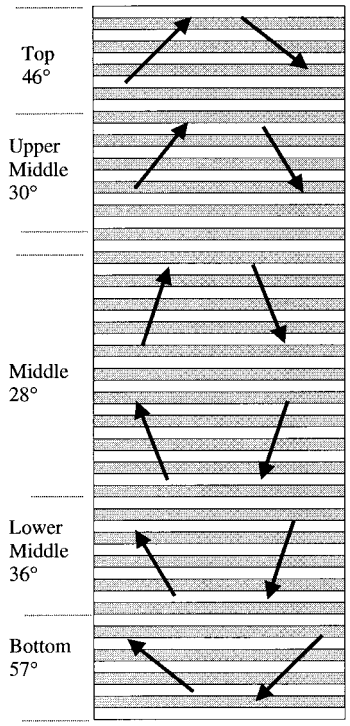

Fig. 2. Depth dependent Mössbauer average angle $\bar{\theta}$ and corresponding sketch of the magnetization distribution in a multilayer with 31 cobalt layers sandwiched by gold (all layers 20 Å thick). Data from the experiments of Hamada *et al.*, references [6,7].

2 Numerical

The code used minimizes the torque associated with the effective field acting on the magnetization: $\boldsymbol{\Gamma} = \mathbf{M} \times \mathbf{H}_{\rm eff}$. $\mathbf{H}_{\rm eff}$ is the effective field with contributions from the exchange, bulk anisotropy, applied and demagnetizing field

energy terms. At each iteration step the magnetization is slowly rotated towards the effective field direction. This method, neglecting the precession, only describes equilibrium states which are said to be reached when the reduced torque $\| \boldsymbol{\Gamma}/2\pi M_\mathrm{S} \|$ is everywhere smaller than 10^{-4} times the anisotropy field $H_K = 2K/M_\mathrm{S}$.

2.1 Discretization

The periodic stripe domains are assumed to be elongated along the OZ-axis. Therefore, the three components of the magnetization vector $\mathbf{m}(\mathbf{r}) = \mathbf{M}(\mathbf{r})/M_\mathrm{S}$ do not depend on the Z coordinate. This axis will be termed longitudinal. In the XOY-plane (see geometry in Fig. 1) Y will denote the film normal – and will be called normal axis –, whereas direction X will be referred to as transverse. In this plane, the continuous magnetization distribution $\mathbf{m}$ is reduced to a finite number of vectors located at the nodes of a regular (Cartesian) grid of periods a and b, limited to one period $2W$ of the magnetic pattern. The a and b parameters are chosen such that the ratios ℓ/a and ℓ/b should remain larger than 5, where ℓ is the smallest characteristic length of the problem: either the Bloch wall width $\pi\sqrt{\frac{A}{K}}$ or the exchange length $\pi\sqrt{\frac{A}{2\pi M_\mathrm{S}^2}}$. Moreover, in the first part of the discussion (Sect. 3) five prisms at least were used to describe the thickness of each individual magnetic layer so that the mesh is fine enough to reflect the variation of $\mathbf{m}$ along OY and allows for a correct implementation of appropriate boundary conditions at the interfaces.

2.2 Surface constraints

In the absence of surface anisotropy and interlayer exchange coupling, the magnetization should be stationary at the interfaces of each magnetic layer ($\partial\mathbf{m}/\partial n = \mathbf{0}$). In the presence of one or both of these contributions, the boundary conditions should be modified accordingly [10]. Only the second contribution will be taken into account in the present work, the thickness of the non magnetic spacer (2 nm) excluding any significant interlayer exchange coupling. Therefore, the surface condition reads

$$\frac{\partial \mathbf{m}}{\partial n} = \frac{K_\mathrm{S}}{A} (\mathbf{n}\cdot\mathbf{m}) [\mathbf{n} - (\mathbf{n}\cdot\mathbf{m})\mathbf{m}], \qquad (1)$$

where K_S is the surface anisotropy constant with easy axis along the normal $\mathbf{n}$ to the layers, and A the bulk exchange stiffness constant. The implementation of such boundary conditions is described in reference [10].

2.3 Demagnetizing field

The calculations use a scheme assuming a constant magnetization within each prism ($a \times b$) leading to charged surfaces [11], and evaluate the average value of the demagnetizing field within each prism. This code was previously adapted [12] in order to take into account the periodic nature of the magnetization distribution ($\mathbf{m}(x, y) = \mathbf{m}(x + P2W, y)$, where P is an integer). Therefore, the period $2W$ is an additional variable in the minimization process. Several calculations differing in the sole $2W$ value have to be undertaken so as to get the lowest energy configuration providing the equilibrium domain period.

In order to save computational time, the following (anti) symmetry with respect to the mid-plane of the sample ($y = 0$) is used: $m_X(x, y) = -m_X(x, -y)$; $m_Y(x, y) = +m_Y(x, -y)$ and $m_Z(x, y) = +m_Z(x, -y)$. This symmetry is obeyed in single films, so that a first justification of this restriction is that we want to compute how bulk-like structures are modified when transposed to multilayers. A second argument applies as soon as the structures develop at a scale larger than the superperiod of the multilayer $2d = 4$ nm, which should hold nearly always as the micromagnetic exchange length Λ is about 5 nm in usual metals. In this regime, charge interaction from layer to layer dominates and forces m_y not to alternate sign from one layer to the next one, like in a single film with nonzero exchange along the normal direction. Then the sign of the component m_x is also fixed by a flux closure argument, again like in single films. Finally, one realizes that the overall sign of m_z in each layer is free (in zero field), as the inspection of the energy terms shows. In all structures shown in the following at $H_z = 0$, one could reverse arbitrarily and independently m_z in all layers without changing the energy. From this, one deduces that M_R and H_C (along the longitudinal axis) could vary a lot in the presence of some defects. However, the magnetic pattern obtained from a saturated state after continuous reduction of the field towards zero, should keep the proposed symmetry. Activation energies are obviously needed to overcome the energy barriers and then to allow a complete freedom of the sign of the m_z component.

3 Detailed study of the $(Co/Au)_{31}$ sample

3.1 Generalities

The numerical simulations were started in order to establish a link with experimental results reported earlier in references [5–7]. This section will be mainly concerned with the analysis of the zero field magnetization distribution of a Co/Au multilayer where the number of ferromagnetic layers in the stack is equal to $N = 31$. The adjusted magnetic parameters used for the present simulations are listed in Table 2. The adjustment was performed on the N dependent experimental results, shown in Figure 7 and discussed in Section 4. The stack is composed of layers alternatively made of cobalt and gold of thickness $d = 20$ Å each (Fig. 1). From X-ray analysis of the crystallographic structure of the multilayers, it turned out that the Co films are polycrystalline in the plane, but mainly hcp(0001) textured along the film normal. This explains the bulk perpendicular anisotropy constant used. Additionally, a

Table 2. Set of parameters for the Co/Au stack used in the micromagnetic simulations of Section 3. The total magnetic thickness relative to twice the Bloch wall width, as introduced by Hubert [13], is also indicated. For single films, the critical thickness is given by $R(Q)$, with $R = 1$ at $Q = 0$ and $R = 0$ at $Q = 1$.

Number of Co layers	$N = 31$
Thickness of one individual layer	$d = 20$ Å
Exchange constant	$A = 3.0 \times 10^{-6}$ erg/cm
Magnetisation	$M_S = 1400$ emu/cm^3
Bulk anisotropy	$K_V = 4.25 \times 10^6$ erg/cm^3
Surface anisotropy	$K_S = 0.425$ erg/cm^2
Effective anisotropy	$K_{eff} = K_V + \frac{2K_S}{d} = 8.5 \times 10^6$ erg/cm^3
Quality factor	$Q = \frac{K_{eff}}{2\pi M_S^2} = 0.69$
Length ratio [13]	$R = \frac{Nd}{2\pi\sqrt{\frac{A}{K_{eff}}}} = 1.66$

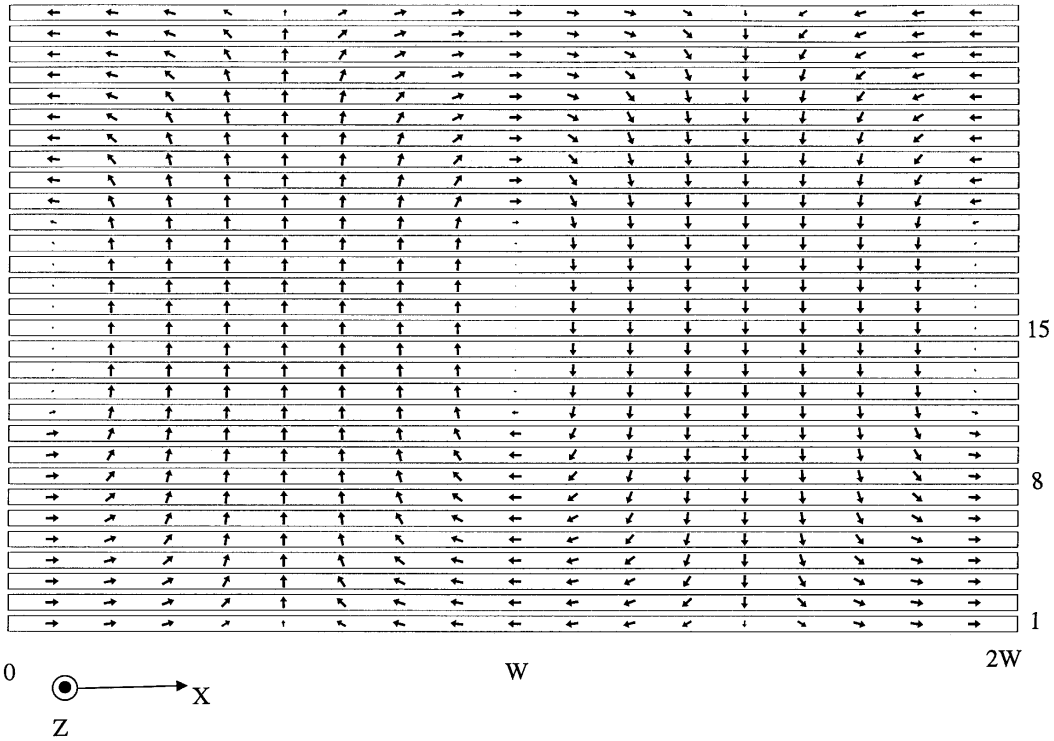

Fig. 3. Cross sectional calculated magnetisation pattern in a $30 \times$ [Co 20 Å/Au 20 Å] multilayer in cross section (the magnetic parameters are given in Tab. 2). The length of arrows is proportional to the modulus of the x-y magnetization components.

surface anisotropy contribution is added *via* the surface anisotropy constant K_S so that the effective anisotropy $K_{eff} = K_V + \frac{2K_S}{d}$ amounts to 8.5×10^6 erg/cm^3. Nevertheless, the quality factor Q ($= K_{eff}/2\pi M_S^2$) remains smaller than 1. Therefore, for one individual Co layer, the magnetization vector stays in-plane under the predominance of the magnetostatic contribution. On the contrary, a "spin reorientation transition" does occur in a stack when increasing the number of magnetic layers N. An increase of N may be viewed as an increase of the total thickness of an effective single film leading to a competition between anisotropy and magnetostatic contributions mainly, the amount of the exchange energy being moderate. In the case $N = 31$, the variation of the $\bar{\theta}$ angles throughout the multilayer, as shown in Table 1, militates in favour of a well-established stripe domain pattern. Such a pattern is drawn in Figure 3 (case $N = 30$) which shows the calculated (cross sectional) magnetization distribution within one optimized period ($2W \approx 260$ nm) of the structure. The length of the arrows is proportional to the

magnetization component in the plane of the figure, *i.e.* $\sqrt{m_x^2 + m_y^2}$. A well defined up and down stripe pattern is visible as well as a pronounced magnetization circulation which considerably reduces the stray field energy. The alternate flux circulation winds around vortices ($m_x = m_y = 0$ and $m_z = +1$) which may be viewed as the core of inner 180° walls between domains. This is especially visible in Figure 4 which gives a more quantitative aspect of the magnetization profiles inside the first (external), eighth and fifteenth (internal) cobalt layers in the stack over one period $2W$ of the structure. One striking feature can be observed in Figure 4b, namely the domain-like rectangular profile of the perpendicular component m_Y especially for the inner layers (*e.g.* 8 and 15). The flux closure or Landau Lifshitz aspect is visible through the variation of the transverse component m_X as shown in Figure 4a, especially for layer 1. Finally, Figure 4c shows that the longitudinal component m_Z keeps a constant sign in each layer, characteristic of the so called "weak" stripe pattern in single films [12]. Notice that for the inner magnetic layers in the stack, the magnetization becomes purely longitudinal ($m_Z = +1$) between the up and down domains.

In the first calculations, five points were put across the thickness of each layer in order to take into account properly the micromagnetic boundary condition in the presence of surface anisotropy. The variation of the magnetization components from bottom to top of one layer is plotted in Figure 5. The presence of surface anisotropy promotes higher values of the normal component in the vicinity of the interfaces of the layer (Fig. 5a) and a corresponding decrease of the in plane components (m_X in Fig. 5b). However, due to the very low variations observed, we have simplified the calculation to one point in the 20 Å thickness while the anisotropy constant used will be now equal to the effective value K_{eff} previously introduced. Such a simplification is well justified on micromagnetic grounds. For example, both characteristic lengths of the problem, the Bloch wall width and the exchange length, are much larger than the thickness of an individual layer. Furthermore, we have carefully checked that these results are very close to the previous ones while, obviously, they come out much faster.

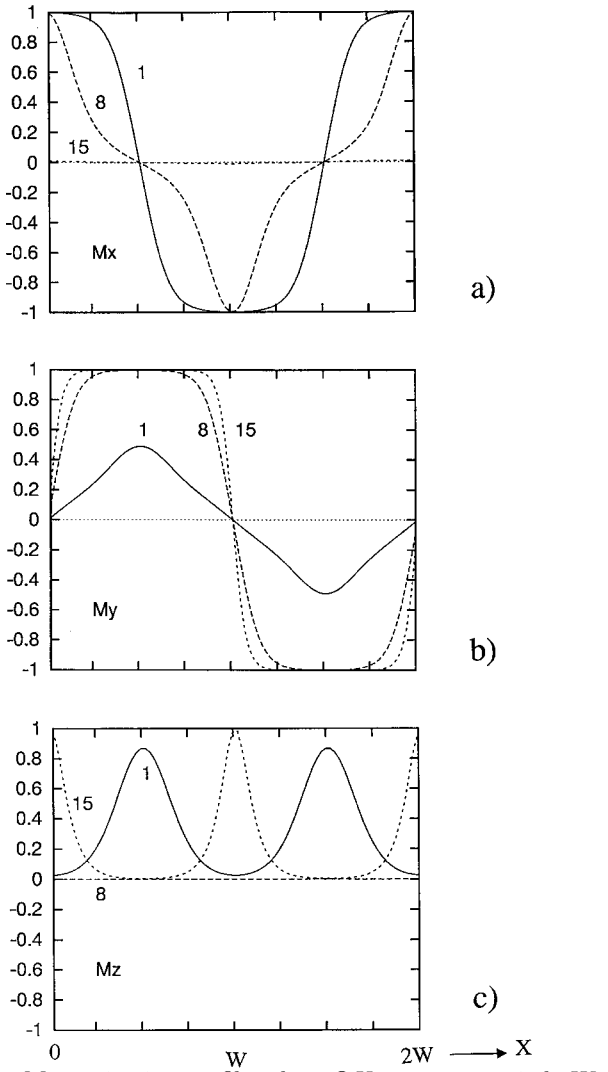

Fig. 4. Magnetization profiles along OX, over one period $2W$, for the first, eighth and fifteenth layer in a stack 30 × [Co 20 Å/Au 20 Å], shown in Figure 3. (a) the transverse m_X, (b) normal m_Y and (c) longitudinal m_Z magnetization components. See comments in the text.

3.2 Experimental versus numerical results

The ability *via* Mössbauer probe layers to investigate the depth dependence of the spin orientation and of the demagnetizing field is of considerable interest. It allows to observe directly the magnetic behavior of individual magnetic layers in the stack and gives important informations on the coupling between layers as well as on the magnetic structure. The experimental values obtained from reference [6] are reported in the central column of Table 3. Various sets of magnetic parameters have been used in order to obtain the best fit with the experimental results available in [6,7], see Section 4. This required to use an exchange constant value of 3×10^{-6} erg/cm, a value already quoted in the literature [1,14]. On the other hand the effective anisotropy constant was fixed to 8.5×10^6 erg/cm^3 which seems in good agreement with other published data by combining a bulk contribution for hcp cobalt $K_{\text{V}} = 4.5 \times 10^6$ erg/cm^3 [15] and a surface anisotropy contribution (it can reach values as high as $K_{\text{S}} = 0.58$ erg/cm^2 [16]). For each calculation, averaged quantities were evaluated according to the nomenclature used in reference [6]: the top (= bottom) area corresponds to the first (last) five layers in the stack, the upper middle (= lower middle) region to the layers 6–10 (22–26) and the middle one to layers 11–20 respectively. The averaged quantities are: $\langle m_Y^2 \rangle = \langle \cos^2 \theta \rangle$ from which an averaged angle $\bar{\theta}$ can be deduced, and the average projected demagnetizing field $\overline{H}_{\text{d}}$ along $\mathbf{m}$ defined as $\overline{H}_{\text{d}} = \langle \mathbf{H}_{\text{d}} \cdot \mathbf{m} \rangle$. Finally, the calculated equilibrium period amounts to $2W = 2604$ Å, equal to the experimental one (from MFM measurements). Table 3 shows

Table 3. Experimental values (from Hamada *et al.*, see Ref. [6]) *versus* numerical results for a multilayer with $N = 31$ cobalt layers. Numerical results pertain to the optimized parameters given in Table 2.

		Experiment	Simulation
Angles (deg.)	Top - Bottom	46–57	54.0
	High - Lower middle	30–36	32.2
	Middle	28	24.6
	⟨average⟩	38	37.1
Demagnetizing field ∥ $H_{\rm d}$ (kOe)	Top	0	3.2
	High - Lower middle	3–4	6.8
	middle	6	7.2
	⟨average⟩	4.6	6.1
Half period, W (Å)		1300	1302

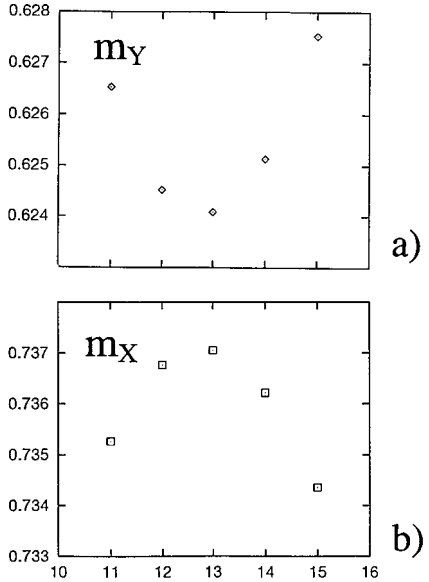

Fig. 5. Variation of the magnetization component across one magnetic layer in the stack (corresponding to the 2nd layer in Fig. 3, from $Y = 42$ Å point 11 to $Y = 58$ Å point 15) for $X = 3W/8$. Plotted are (a) the normal component m_Y, (b) the in-plane of the layer component m_X.

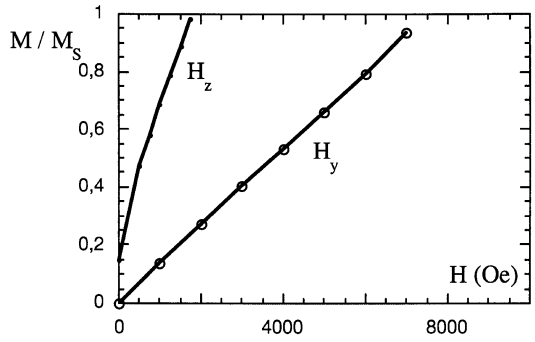

Fig. 6. Simulated initial magnetization curves for an applied field normal (H_Y) to the stack, or in-plane and along the stripes (H_Z), case $N = 31$. The longitudinal remanent magnetization $M_{\rm R} = \langle m_z(H_z = 0)\rangle$ is very low: $M_{\rm R} = 0.15$.

the good agreement between experiments and simulations. The main trends already emphasized in reference [6] are correctly reproduced by the simulation: i) the increase of $\bar{\theta}$ when moving from the middle to the surface of the stack and ii) the corresponding decrease of the demagnetizing field, both effects originating from the multidomain configuration in zero field. However, concerning the angles, the experimental asymmetry observed (values at top $\bar{\theta} = 46°$, bottom $\bar{\theta} = 57°$) cannot be reproduced in the present calculation, where firstly identical magnetic parameters are assumed for all the magnetic layers, and secondly symmetrical structures only are searched.

The calculated demagnetizing fields are always higher than the experimental values extracted from the hyperfine field. However, except at the top and bottom regions, they are still very close to the upper limit of the estimated experimental error of ±2 kG. Note also that in the present simulations the usual bulk magnetization value for cobalt is used ($4\pi M_{\rm S} = 17.59$ kG) whereas the value deduced from Mössbauer measurements amounts to 15.7 ± 1 kG. The difference seems therefore to be systematic.

The magnetization curves were also calculated. They are shown in Figure 6 for an applied field either normal to the stack (H_Y) or longitudinal (H_Z). The shapes of the $M(H)$ curves are in good agreement with the experimental ones [7], especially for the perpendicular case. However, the longitudinal saturation field obtained so far is lower than the experimental one, and the approach towards saturation differs: the slope of the calculated $m_Z(H_Z)$ curve is much higher than the experimental one. This might result from differences in the properties of the layers, as suggested above, or from domain effects (see Fig. 7). Finally, a magnetic energy calculation was performed. The different energy contributions, normalized to $E_{\rm D} = 2\pi M_{\rm S}^2$, for the equilibrium stripe pattern in zero applied field amount to: exchange $E_A/E_{\rm D} = 0.023$, anisotropy $E_K/E_{\rm D} = 0.251$, demagnetizing $E_{\rm d}/E_{\rm D} = 0.337$, the corresponding total magnetic energy being $E/E_{\rm D} = 0.612$ (indeed lower than the value $E/E_{\rm D} = Q = 0.69$ for the purely in-plane structure). This calculation shows that the exchange contribution is very low while the demagnetizing term provides the highest contribution as assumed in reference [7].

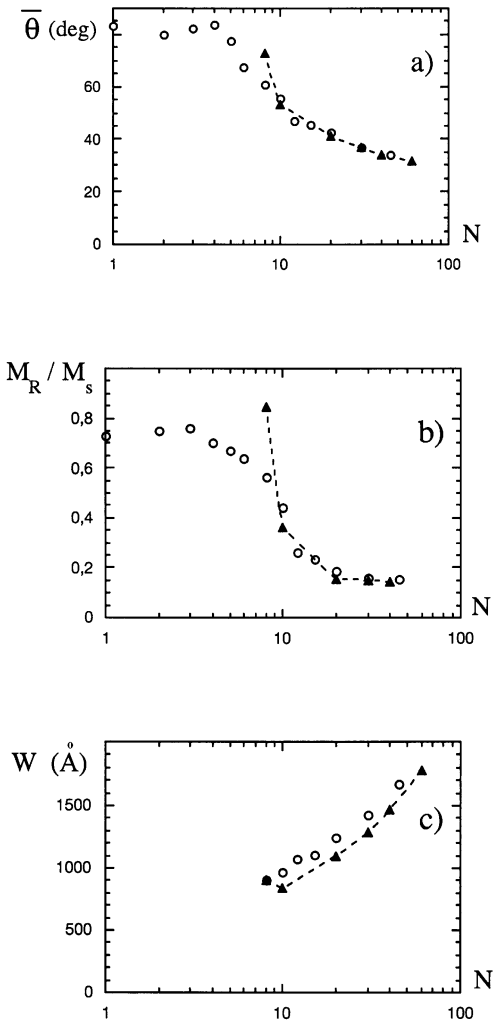

Fig. 7. N-dependent experimental (o, from Refs. [6,7]) and simulated (-- ▲ --) global parameters of the $[Co/Au]_N$ samples: (a) the average angle between M and the normal to the stack, (b) the in plane longitudinal remanent magnetization under zero applied field and (c) domain width (half period). Optimized magnetic parameters were used (see text for details).

4 Evolution of the magnetic structure and parameters of the $[Co/Au]_N$ multilayers with increasing N (experiment vs. simulations)

Several calculations, using different sets of magnetic parameters, have been performed in order to obtain the best fit with the experimental data published in references [6,7]. The numerical parameters that resulted are those used in Section 3.2: $A = 3 \times 10^{-6}$ erg/cm, $K = 8.5 \times 10^6$ erg/cm^3 and $M_S = 1400$ emu/cm^3 giving $Q = 0.69$. The final results of these simulations are gathered in Figure 7, which shows the good agreement with experiments that could be obtained. For a number of magnetic layers lower than $N = 7$, the magnetization stays in the plane of the stack, which corresponds to $\bar{\theta} = 90°$ with a remanent longitudinal magnetization $M_R/M_S = 1$. Experiments do not show a full remanence, but rather a value about 0.75. This reduced value may well arise from domains forced by the finite size of the sample.

At $N = 8$ a weak stripe pattern is predicted to appear, with a domain width of $W = 900$ Å. Such results can be compared to what is expected for a single film with the same magnetic parameters and a quality factor $Q = 0.69$. From the phase diagrams found in [13] describing the transition between a single domain and a stripe pattern, as a function of the thickness of the film and under an applied field, the minimum thickness for the appearance of a stripe pattern (in zero field) amounts to 155 Å. This is not so far from the total effective thickness of the seven magnetic layers 20 Å thick each. On the other hand, the critical domain width in the case of a thin film is equal to 390 Å, a value strongly different from the 900 Å observed for the multilayer.

The critical thickness and critical domain period result from a delicate balance of anisotropy with demagnetizing and exchange energies, the demagnetizing term being often more important [17]. This balance is altered by multilayering. For example, the 160 Å single film located just above nucleation has $E_K/E_D = 0.663$, $E_d/E_D = 0.019$ and $E_A/E_D = 0.007$ (sum 0.689 just below $Q = 0.69$). For the corresponding multilayer at $N = 8$ these values become 0.625, 0.055 and 0.009, respectively. One observes that the relative weight (w.r.t. the demagnetizing term) of the exchange E_A/E_d has decreased, as anticipated from the disappearance of exchange interaction across the y-direction. Following previous work [8], nucleation of the non-uniform structure occurs at the thickness where the lowest eigenvalue of the energy functional is zero. The eigenvalues are those of the energy for infinitesimal m_x and m_y. A zero eigenvalue means that the cost in demagnetizing and exchange energies is just compensated by the gain in anisotropy. The following argument can be used to understand the effect of multilayering on the micromagnetic configurations. Take a configuration at nucleation in a single film. Dilate all lengths by a factor of 2. The densities of anisotropy and demagnetizing energy do not change (they involve no length scale) in this process, whereas the exchange one falls to a quarter. The result is a bit subtle for the demagnetizing term. First, it can be proved mathematically that this energy density is invariant under a dilatation of all dimensions by the same factor (the factor has to be unique, think of the divergence term). Alternatively, in order to make the result more intuitive, one can recall that the demagnetizing factors of the body depend on its shape, but not on its absolute size. As the configuration at nucleation is rather smooth, the energy densities (in terms of magnetic volume) again do not change when half of the material is removed through N slices, especially if N is large. There is a small increase of the demagnetizing term because of the additional poles that appear at the interfaces, counterbalancing the exchange energy decrease. Altogether, a configuration at nucleation in a single film, when dilated by 2 and then reduced by 2 through slices, keeps an energy cost close to zero. Neighbouring configurations (with other

periods) also keep nearly their energy densities, which are positive. Thus, the rule of thumb is that the critical thickness will be the same, in terms of magnetic material, as for a single film, while the critical domain period doubles. This is reasonably close to the numerical results shown before. Note finally that the argument is not restricted to the case where magnetic and non-magnetic thicknesses are equal. It has been confirmed by test calculations in the case of gold layers twice as thick. The general argument exposed before predicts that the period at nucleation should triple, which is what these calculations found.

Beyond $N = 8$ the reorientation transition of the Co magnetization is clearly observed through the decrease of the average angle $\bar{\theta}$ and the drop of $M_{\rm R}$. The domain period increases with thickness following the well-known Kittel law $W \propto \sqrt{N}$ for films with perpendicular magnetization [18].

5 Analysis of the N dependent magnetic structure for varying Q factor

5.1 Generalities

A more general approach is developed in the following which considers both the number of magnetic layers N in the stack and the Q factor of the material used. The discussion starts with the diagram of Figure 8a showing the N dependent remanent longitudinal magnetization $\langle m_Z \rangle$ (average value over one period of the structure). The magnetic parameters used in this section are $A = 1.8 \times 10^{-6}$ erg/cm, $M = 1430$ emu/cm^3 while the anisotropy constant varies from $8{\times}10^6$ to $1.2{\times}10^7$ erg/cm^3 which corresponds to parameters often found in the literature for cobalt (note that we keep $Q < 1$). The discussion is restricted to a stack composed of magnetic layers and non magnetic spacers all 20 Å thick. For a low number of magnetic layers, the magnetization stays in the plane of the layers, which corresponds in the figure to $\langle m_Z \rangle = 1$. This can be interpreted as the existence of a critical number of layers (critical thickness in case of one individual layer) below which no stripe exists. The critical number of layers increases with decreasing value of the quality factor: $N = 2$, 4, 6 and 9 for $Q = 0.93$, 0.78, 0.70 and 0.62 respectively as shown in Figures 8a and 8b. A comparison with the behavior of a single magnetic film is given in Figure 9 in the case $Q = 0.7$. The critical parameters for several Q values (thickness t and domain half-period W) are gathered in Table 4 and compared to values for single films [19,20]. The same general remarks as given previously apply: the critical thickness above which a stripe pattern occurs in a continuous film is of the order of the corresponding total thickness of the magnetic layers ($N \times 20$ Å). However, at the appearance of the stripe pattern, the magnetic period $2W$ is much higher (nearly twice, as explained above) in the case of a multilayer than in a single film. One should note on Figure 9a another characteristic of the magnetization pattern in multilayers: the longitudinal component is greatly reduced compared

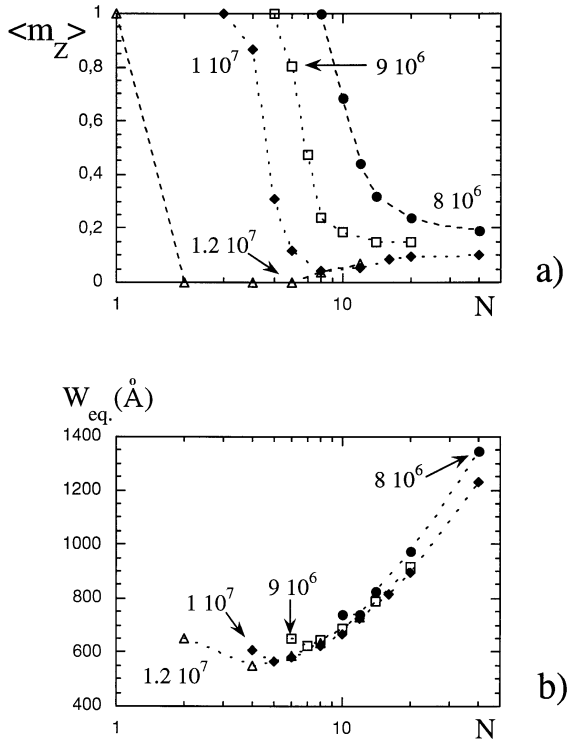

Fig. 8. Variation of: (a) the longitudinal remanent magnetization component ($M_{\rm R}/M_{\rm S} = \langle m_Z \rangle$) and (b) the domain width W, *versus* the number of magnetic layers N and for different values of the anisotropy constant K indicated in the figure and corresponding to quality factors of $Q = 0.62$ (-●-), 0.7 (-□-), 0.78 (-♦-) and 0.93(-△-) .

to a single film. This occurs because of the absence of the exchange coupling in the normal direction. In a single film this interaction propagates the core of the vortices that exist in the middle of the domain walls. For an even number of layers the vortex core even disappears. For an odd layer number this core remains in the central layer, due to symmetry (see Sect. 2.3, it may well disappear also in that case in calculations without assumed symmetry).

The monotonous decrease of the remanent in-plane magnetization $\langle m_Z \rangle$ with increasing N, that was seen in Figure 7b, is not a universal behaviour as revealed in Figure 8a. For large values of the anisotropy constant ($1{-}1.2 \times 10^7$ erg/cm^3), the longitudinal remanent component $M_{\rm R}$ decreases abruptly with increasing N, then goes through a minimum and finally slightly increases towards a plateau.

After nucleation, the shape of the $W(N)$ curves in Figure 8b follows the general behaviour already mentioned in the pioneering work of Malek and Kambersky [21] on a single layer, and experimentally observed in Co/Pt multilayers [2]. The width of the domain W begins to decrease with increasing N. After reaching a certain minimum value the period of the stripe then increases following the Kittel law: $W \propto \sqrt{N}$ [18]. Let us notice that the equilibrium periods found are lower than observed experimentally (compare Figs. 7c and 8b), the difference coming mainly from the different exchange constants A used in Sections 4 and 5.

Table 4. Estimated critical parameters (thickness and domain width W) at the nucleation of a stripe pattern for a single film and corresponding values calculated for a multilayer (see text) with $A = 1.8 \times 10^{-6}$ erg/cm $M_S = 1430$ emu/cm^3 and various values of the anisotropy.

	Single film		Multilayer	
Q factor	critical thickness (Å)	domain width W (Å)	magnetic layers number N	domain width W (Å)
0.62	149.2	324.0	9	755
0.7	117.0	300.0	6	650
0.78	92.8	357.0	4	600
0.93	38.4	427.0	2	650

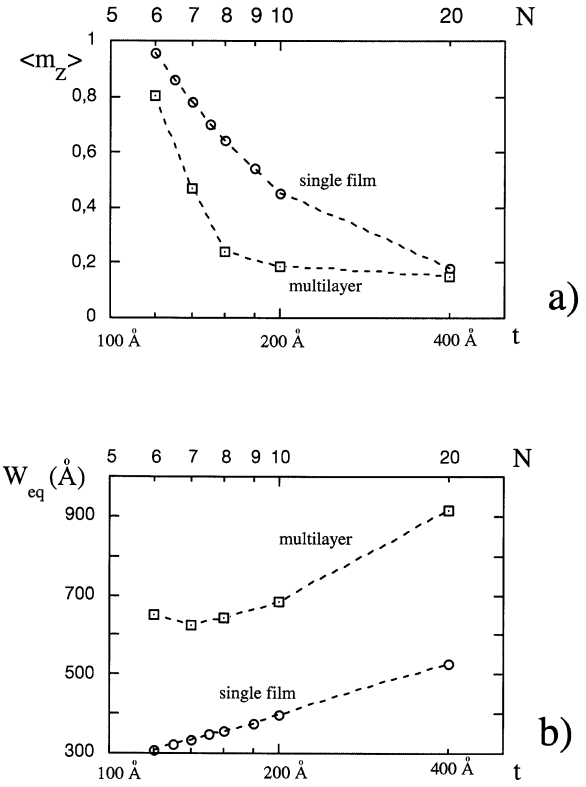

Fig. 9. Variation of: (a) the longitudinal remanent magnetization component ($M_R/M_S = \langle m_Z \rangle$) and (b) the domain width W, *versus* the number of magnetic layers N in a multilayer or the thickness of one single film t, with the convention $t(\text{Å}) = N \times 20$ Å. This figure corresponds to the case $Q = 0.7$.

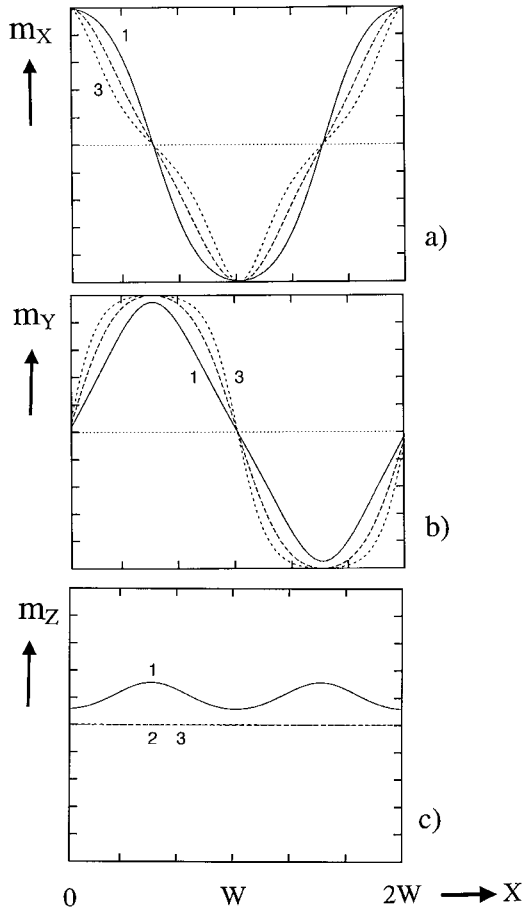

Fig. 10. Magnetization profiles over one period $2W$ across the first three layers in a $6\times$[Co 20 Å/Au 20 Å] multilayer with $A = 1.8\times10^{-6}$ erg/cm, $K = 10^7$ erg/cm^3 and $M = 1430$ emu/cm^3. (a) m_X, (b) m_Y and (c) m_Z components.

5.2 Q factors close to 1

At the beginning of the ripening of the stripe pattern the magnetization (especially that of the inner layers) lies preferentially in the transverse plane (XOY). This is illustrated in Figure 10 showing the magnetization distribution across one period ($2W$) of the stripe pattern, for half of the six layers in the stack considered [the distribution in the other layers being obtained by symmetry: (i) → (7-i)]. The longitudinal in plane component m_Z is equal to zero in the inner layers numbered 2 and 3 over all the period of the pattern. Only the external layer 1 exhibits a moderate m_Z value. A single film of equivalent thickness would have a much higher longitudinal component (see Fig. 9a).

In order to gain more information about the nucleation process we studied the evolution with N of the local m_Z component across the N layers of the stack, in the centre of the wall between the main "up" and "down" domains. In the case of a single magnetic film, the z component of the reduced magnetization m_Z is strictly equal to 1 in the middle of the film and then decreases continuously when approaching both surfaces in order to allow, more or less,

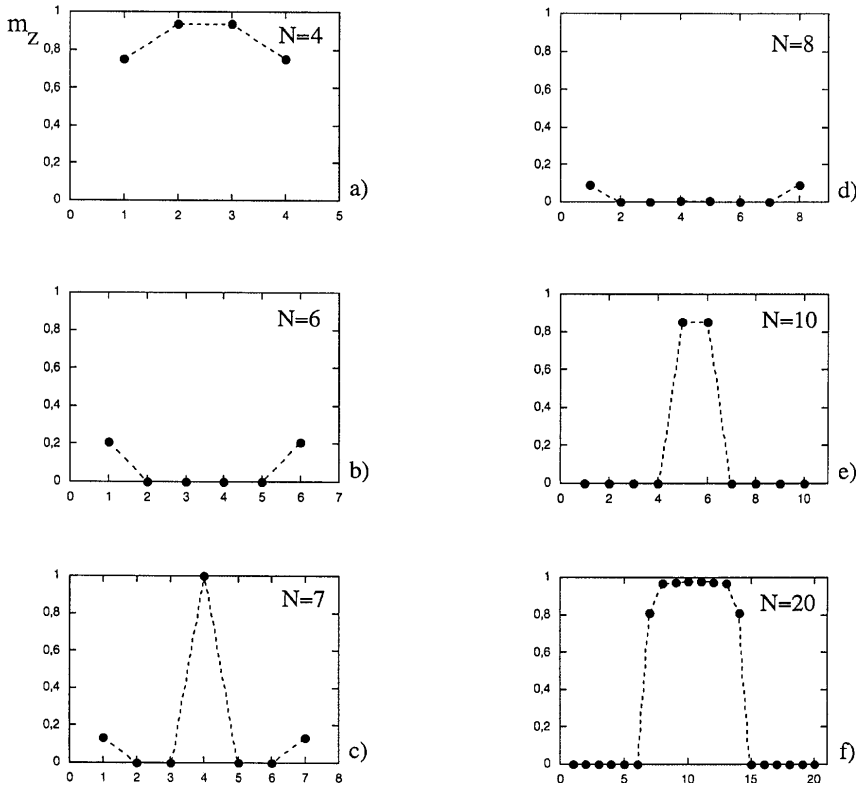

Fig. 11. Variation of the longitudinal m_Z component across all the layers of the stack (top to bottom) at the core of the main walls in the case of an anisotropy constant equal to $K = 10^7$ erg/cm^3. The parameter N corresponds to the number of magnetic layers in the stack.

the flux closure inside the sample [22]. For multilayers, excluding the cases of an odd number of magnetic layers where the symmetry used imposes also $m_Z = 1$ in the middle of the stack (*e.g.* case $N = 7$ in Fig. 11), such a behaviour is only visible at the very beginning of the nucleation of the stripes (*e.g.* $N = 4$ in Fig. 11). Remind that in this calculation, the magnetization is assumed uniform across the layer thickness. Therefore, the dashed lines in Figure 11 only give a schematic overview of the evolution of this component across the stack. The large variation of m_Z from one magnetic layer to the adjacent one is clearly the result of the discontinuous aspect of the multilayer enhanced by the absence of any interlayer (ferromagnetic) exchange coupling. When increasing the number of magnetic layers in the stack ($N = 6$ and 8 in Fig. 11) the longitudinal component either disappears or is largely reduced. It turns out that between the two main magnetization distributions possibly adopted by the system and schematically depicted in Figure 12 (Bloch or split-Néel), the second one (Fig. 12b) is the one observed: the wall structure exhibits essentially a Néel aspect. Systematic analysis has shown this to occur when the following conditions are achieved: i) the main domains (essentially up and down) are sufficiently formed or Q is large (but still lower than unity), ii) the number of layers N is not too large and iii) each layer (20 Å here) is much thinner than any characteristic length ℓ. Such a situation is mainly governed by the dipolar effect. A similar behavior was already described in [1] where 2D micromagnetic wall structure calculations were performed on a $10\times$[Co(3.5 Å)/Pt(10.5 Å)] multilayer.

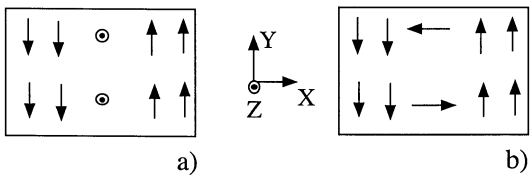

Fig. 12. Schematic magnetization distribution over one period $2W$ of the pattern in the case of a moderate number of layers in the stack, and a sufficiently large anisotropy constant. The main up and down domains are separated by: (a) Bloch-like walls and (b) Néel-like walls ensuring a reduction of the stray field energy.

Finally, increasing N further ($N = 10$, 20 in Fig. 11) leads to the reapparition of the vortices ($m_x = m_y = 0$ and $m_z = +1$), with the conventional inner flux circulation around them. They may be viewed as the core of inner 180° Bloch walls between domains, already described previously and shown in Figures 4 and 12a. Such structures are very similar to Bloch walls in bulk samples, with their Néel caps. In Figure 8a one sees that for large values of N the longitudinal remanent magnetization M_R still differs from zero for all values of the anisotropy constant used. This corresponds to the contribution of the Bloch wall cores. A rough estimate of the M_R value is δ/W, where δ is the wall width. The apparent constant value of M_R

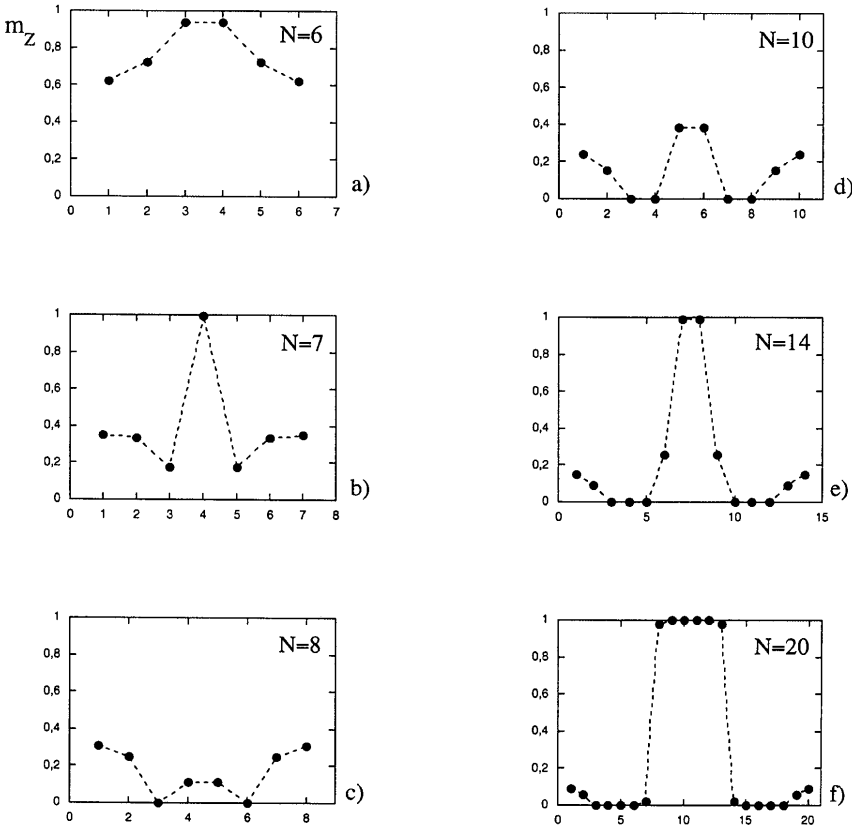

Fig. 13. Same as Figure 11 but for $K = 9 \times 10^6$ erg/cm^3.

at large N means that δ is not constant, but rather scales as $N^{1/2}$, like W.

We have thus seen three regimes for N: in-plane saturation at low values, domain-like behaviour with split Néel walls at intermediate values, and finally domains with Bloch walls. Experiments [7] had also put forward three regimes, the distinction between the second and third being based on the slope of the $\bar{\theta}(N)$ curve. Calculations find the same feature (Fig. 7b), and provide a qualitative distinction between these two regimes.

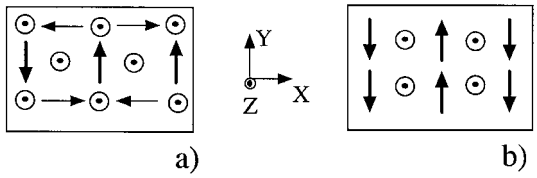

Fig. 14. Schematic drawing of the magnetization distribution in cross section (XOY plane) in the case of a film exhibiting weak stripes with: (a) a low quality factor and (b) a high one.

5.3 Lower Q factors

For a moderate value of the anisotropy constant (*e.g.* $K \leq 9 \times 10^6$ erg/cm^3) a regular decrease of $\langle m_Z \rangle$ is observed with increasing N till a plateau is reached. The corresponding magnetization profiles (see Fig. 13), appear more complicated than in the previous case with higher anisotropy. Near the external surfaces of the stack (1st and Nth layers) the longitudinal component decreases continuously from 1 to 0 with N. However, the decrease of m_Z in the inner layers of the stack is much more pronounced. Therefore, very surprising situations may occur like for example the case $N = 10$ (Fig. 13d) where the longitudinal component exhibits three maxima located at the inner 5th and 6th but also extreme 1st and 10th layers (see also Ref. [3]). It seems that the dipolar coupling or the flux circulation is restricted to the inner layers while the individual behaviour of each layer at the two surfaces of the stack (1st and 10th) is preserved. Under such an hypothesis, as one individual layer alone is not thick enough to support a normal magnetization, one understands the higher values of m_Z observed (see also Fig. 10c). Another cause for the increased longitudinal magnetization is explained in Figure 14, which compares the schematic structures of weak stripes in lower and higher anisotropy samples.

6 Conclusions

2D numerical simulations of stripe domains in magnetic multilayers have been performed. A nice agreement has been found with available experimental results on $[\mathrm{Co/Au}]_N$ stacks. Using a reasonable set of magnetic parameters the experimental data (remanent magnetization, stripe periodicity and average angle $\bar{\theta}$) were correctly

reproduced numerically as a function of the number N of layers in the stack.

Compared to a single film, the nucleation of a stripe pattern in multilayers exhibits two main differences. In terms of the critical thickness needed for a continuous film to nucleate stripe domains, the total amount of magnetic material (N times the thickness of one individual layer) in the stack is quite similar. Such is not the case for the equilibrium domain period, much higher in the case of a multilayer than that for a continuous medium. This effect was shown to be mainly due to the modification of the dipolar energy by layering.

The second major difference is related to the magnetization profiles. Two different states have been described during the development of the stripe pattern in a multilayer. For a moderate but sufficient number of layers, the magnetic pattern is characterized mainly by a succession of "up" and "down" domains. In between domains, the wall structure is characterized by its Néel aspect which allows the flux closure inside the stack. Therefore the sense of rotation of $\mathbf{m}$ reverses abruptly at the center of the stack from one layer to the adjacent one (split Néel walls). Such opportunity never occurs in a single film because the exchange penalty involved in such process would be too high. On the contrary, the presence of Néel-like section of walls with opposite polarities at top and bottom surfaces may be observed for a monolayer medium. However, in this case, there is always an intervening Bloch-like section through the center of the film leading to the well known vortices (or vortex walls). What we described in the last section is that this opportunity also occurs for a multilayer, but above a second threshold value for N corresponding to the onset of a vortex.

This work, although limited to the case where magnetic and non magnetic thicknesses are equal (to 20 Å) and with no indirect exchange coupling between magnetic layers, already demonstrates the richness of the magnetic structures in a multilayer sample.

We thank Prof. T. Shinjo and Dr. S. Hamada from the Institute for Chemical Research, Kyoto University, Japan, for communicating their results prior to publication and for many valuable discussions that inspired this work.

References

1. R. Ploessel, J.N. Chapman, M.R. Scheifein, J.L. Blue, M. Mansuripur, H. Hoffmann, J. Appl. Phys. **74**, 7431 (1993).
2. L. Belliard, J. Miltat, V. Kottler, V. Mathet, C. Chappert, T. Valet, J. Appl. Phys. **81**, 5315 (1997).
3. M. Labrune, L. Belliard, Phys. Stat. Sol. (a) **174**, 483 (1999).
4. S. Honda, Y. Ikegawa, T. Kusuda, J. Magn. Magn. Mater. **11**, 273 (1992).
5. S. Hamada, N. Hosoito, T. Shinjo, J. Phys. Soc. Jpn **66**, 30 (1997).
6. S. Hamada, N. Hosoito, T. Ono, T. Shinjo, J. Mag. Soc. Jpn **22**, 405 (1998).
7. S. Hamada, N. Hosoito, T. Shinjo, J. Phys. Soc. Jpn **68**, 1345 (1999); S. Hamada, N. Hosoito, T. Ono, T. Shinjo, J. Magn. Magn. Mater. **198-199**, 496 (1999).
8. R.W. Muller, Phys. Rev. **122**, 1485 (1961).
9. M. Labrune, J. Miltat, G. Traeger, A. Hubert, *Proceedings of the ICMFS Conference* (The Institute of Physics, London, 1991), p. 388.
10. M. Labrune, J. Miltat, J. Magn. Magn. Mater. **151**, 231 (1995).
11. P. Trouilloud, J. Miltat, J. Magn. Magn. Mater. **66**, 199 (1987).
12. M. Labrune, J. Miltat, J. Appl. Phys. **75**, 2156 (1994).
13. A. Hubert, R. Schäfer, *Magnetic domains* (Springer, Berlin, 1998), p. 301.
14. R.H. Victora, J. Appl. Phys. **62**, 4220 (1987).
15. S. Chikazumi, *Physics of magnetism* (J. Wiley & Sons, 1968).
16. V. Grolier, J. Ferré, A. Maziewski, E. Stefanowicz, D. Renard, J. Appl. Phys. **73**, 5939 (1993).
17. V. Kambersky, J. Magn. Soc. Jpn **19-S1**, 37 (1995).
18. C. Kittel , Phys. Rev. **70**, 965 (1946) .
19. N. Vukadinovic, O. Vacus, M. Labrune, O. Acher, D. Pain, Phys. Rev. Lett. **85**, 2817 (2000).
20. N. Vukadinovic (private communication).
21. Z. Malek, V. Kambersky, Czechosl. J. Phys. **8**, 416 (1958).
22. A. Hubert, IEEE Trans. Mag. **21**, 1604 (1985).